Journal of Nuclear Materials 462 (2015) 382–390

Contents lists available at ScienceDirect

Journal of Nuclear Materials

journal homepage: www.elsevier.com/locate/jnucmat

Helium bubbles in bcc Fe and their interactions with irradiation

Xiao Gai *, Tomas Lazauskas, Roger Smith, Steven D. Kenny

Department of Mathematical Sciences, Loughborough University, Leicestershire LE11 3TU, UK

ARTICLE INFO

Article history:
Available online 11 November 2014

ABSTRACT

The properties of helium bubbles in a body-centred cubic (bcc) Fe lattice have been examined. The atomic configurations and formation energies of different He–vacancy complexes were determined. The 0 K results show that the most energetically favourable He to Fe vacancy ratio increases from about 1:1 for approximately 5 vacancies up to about 4:1 for 36 vacancies. The formation mechanisms for small He clusters have also been considered. Isolated interstitials and small clusters can diffuse quickly through the lattice. MD simulations of randomly placed interstitial He atoms at 500 K showed clustering over the time scale of nanoseconds with He clusters containing up to 4 atoms being mobile over this time scale. He clusters containing 4 or 5 atoms were shown to eject an Fe dumbbell interstitial which could then detach from the He cluster and diffuse with the remaining He–vacancy complex being effectively immobile. Collision cascades initiated near larger bubbles showed that Fe vacancies produced by the cascades readily become part of the He–vacancy complexes. Energy barriers for He to join an existing bubble as a function of the He–vacancy ratio are also calculated. These can be larger than the diffusion barrier in the pristine lattice, but are lower when the bubbles contain excess vacancies, thus indicating that bubble growth may be kinetically constrained.

1. Introduction

Reduced-activation ferritic/martensitic steels are candidate materials for use in nuclear reactors [1,2]. The presence of transmutation-created helium plays an important role in the microstructural evolution of these steels under neutron irradiation. Interstitial helium atoms increase the production of Frenkel pairs whilst substitutionals tend to decrease this production [3].

Small helium–vacancy clusters may play an important role in the nucleation of He bubbles. Helium bubbles will cause additional swelling and embrittlement [4,5]. Helium effects on microstructural evolution in tempered martensitic steels were characterised using a novel in situ He-implanter technique by Yamamoto et al. [6] combined with neutron irradiation at 500 °C. Most bubbles that formed had diameters of less than 2 nm.

Ono [7] has studied the formation and migration of He bubbles in high purity Fe and Fe–9Cr ferritic alloy by in situ transmission electron microscopy (TEM) observation, which shows bubbles preferentially form at dislocations in both materials at 200–400 °C. The size distributions of bubbles formed at 400 and 600 °C were compared to show that adding Cr could reduce the diffusion of He. Some bubbles that were not formed at dislocations, were shown to grow in size at elevated temperatures and the motion of small bubbles ($\lesssim$3 nm diameter) was observed over periods of seconds in pure Fe at 750 °C. However the energy barrier for this motion to occur is very large, of the order of 3.5 eV.

Work by Henry et al. [8] demonstrated the effect of helium on the fracture properties of a 9Cr martensitic steel. The size of He bubbles observed in the TEM micrograph was of the order of 0.5 nm in diameter and this small size was attributed also to the influence of Cr inhibiting bubble growth. Finally experimental work from Yu et al. [9] in pure Fe at room temperature has indicated that there is a distribution of sizes with a fairly narrow spread and a preferred He bubble size of the order of 1.5 nm in diameter.

The conclusion of the experimental work is therefore that the bubbles in Fe prefer to remain small at room temperature and especially so when chromium is added to the matrix. When the temperature is increased then smaller numbers of larger bubbles are formed.

However, the atomistic properties of He in metals are difficult to identify experimentally. Thus atomistic simulations such as molecular dynamics (MD) and Kinetic Monte Carlo (KMC) provide useful tools to study the formation and the stability of these clusters.

Because of the significance of the He bubble problem, there has been much recent work on atomistic modelling and developing interatomic potentials to model dynamical processes involving He in metals. Caro et al. [10,11] investigated the properties of

* Corresponding author.
E-mail address: X.Gai@lboro.ac.uk (X. Gai).

http://dx.doi.org/10.1016/j.jnucmat.2014.10.027
0022-3115/

helium bubbles in Fe and FeCr alloys, mainly focussing on their dimensions and determining the bubble pressure. Gao et al. [12] carried out atomistic simulation to examine the clustering of helium in bcc iron and the growth of an helium bubble in helium-rich, vacancy-poor conditions. It was shown that a 1/2 ⟨1 1 1⟩ dislocation loop is formed as a sequential collection of ⟨1 1 1⟩ crowdions, the latter being the most stable self-interstitial atom configuration in the presence of an over-pressurised He cluster. Di et al. [13] found that helium bubbles in Au preferentially nucleate at screw dislocation nodal points and result in helium bubble superlattice formation, which is completely isomorphic with the screw dislocation network along the twist-grain boundary. Stoller and coworkers [14,15] developed a three body He–Fe potential and investigated the pressure and compressibility for He–vacancy clusters. Bubble size, He content and temperature effects were also investigated based on this potential [16]. It was found that the equilibrium He content is rather low and at a room temperature it is ~0.38–0.5 He per vacancy for bubble diameters from 1 to 6 nm. However this was calculated by assuming that the bubble size was such as to induce no strain in the lattice.

Jourdan and Crocombette [17] proposed a variable-gap energy model for helium bubbles in Fe, based on MD calculations to determine quantities such as binding energies, solid to fluid transition and helium density in the bubbles.

Hafez Haghighat and Schäublin [18] investigated the basic mechanisms of the interaction between a moving edge dislocation and a void or He bubble, as a function of its He content, temperature and interaction geometry by MD simulations. The results show that the He bubble induces an inhomogeneous stress field in its surroundings, which strongly influences the dislocation passage depending on the geometry of the interaction.

Hayward and Deo [19] investigated He–H bubbles to examine the synergistic effect between H and He and were able to show that this synergy arose as a consequence of bubble growth through helium induced loop punching, aided by the presence of hydrogen, instead of as a direct interaction between hydrogen and helium.

Terenyev et al. studied the diffusivity of small helium–vacancy clusters and pure He clusters and also investigated the dissociation energies for the He–vacancy clusters [20]. Hepburn performed first-principles study to show the binding of additional He and vacancies to existing clusters could lead to unbounded growth [21].

Yang et al. [22] considered the nucleation of He bubbles at 800 K in bcc Fe using a methodology similar to that described here. They were able to conclude that He would diffuse with a low energy barrier of 0.06 eV rapidly forming small clusters that in turn could also diffuse and that He_4 clusters could emit an Fe interstitial and bind with a vacancy. This process is sometimes termed 'trap mutation' in the literature. However once an He_n cluster formed with a vacancy it became effectively immobile. This was followed by work by Gao et al. [23] who investigated the properties of single vacancy clusters (He_nV). The results show that at 300 K the He_nV cluster is stable up to $n = 6$ and up to $n = 16$, the He_nV_2 cluster is stabilised by the emission of an Fe interstitial in the form of a ⟨1 1 0⟩ dumbbell.

In this paper, the results of a study both on the statics of small helium–vacancy clusters in bcc iron and their interaction with nearby collision cascades are presented, which will provide insight into how an helium bubble forms and grows. We also investigate the structure of small He clusters in Fe and the energy barriers that need to be overcome before growth by diffusion can occur.

2. Computational method

Choosing a good potential to represent the atomic interactions is crucial. Several potentials have been developed to be used to describe the atomic interaction of the helium–vacancy clusters in the bcc Fe system. The Fe–He potential employed here is a many-body potential developed by Gao et al. [24]. The Ackland and Mendelev potential (AM-potential) is used for the Fe–Fe interactions [25]. To describe the He–He interactions, we use the Aziz helium potential [26].

2.1. He bubble formation energies

The formation energy of an He–vacancy complex He_nV_m (n He in m Fe vacancies) is defined [27] as the difference in total energy between a crystal containing a defect and a perfect crystal of the same number of Fe atoms with the corresponding number of helium atoms in their lowest energy structure. This structure was determined by using a Monte Carlo algorithm [28]. It assumes that the He atoms are located in pre-existing vacancies in the bcc Fe system.

$$E_f = E_b + (n-m)E_{\text{vac}} - N_{\text{Fe}}E_{\text{Fe}} - nE_{\text{He}}^{\text{sub}}, \tag{1}$$

where E_f is the formation energy; E_b is the energy of the lattice containing the bubble; E_{vac} is the formation energy of a single vacancy in bcc Fe lattice, defined as follows;

$$E_{\text{vac}} = E(v, N-1) - (N-1)E_{\text{Fe}}, \tag{2}$$

where $E(v, N-1)$ is the energy of the lattice containing one vacancy, $N-1$ is the number of Fe atoms in the system.

N_{Fe} is the number of Fe atoms in the lattice containing the bubble; E_{Fe} is the cohesive energy of Fe and $E_{\text{He}}^{\text{sub}}$ is the energy of a helium substitutional atom, defined as follows,

$$E_{\text{He}}^{\text{sub}} = E_{\text{sub}}^{\text{ref}} - N_{\text{Fe}}^{\text{ref}}E_{\text{Fe}}. \tag{3}$$

It the difference in energy between a perfect lattice with an He atom at infinity and the same one that has an Fe atom replaced by the He, i.e. the energy difference from replacing an He atom at infinity with an Fe atom at infinity.

In the calculations for the formation energy, the box size is set to $30a_0 \times 30a_0 \times 30a_0$, where a_0 is the bcc Fe lattice parameter. For all calculations periodic boundary conditions and constant volume are used. The Monte Carlo algorithm used to determine the lowest energy configuration of the cluster [28] is organised as follows. First, the energetics of voids without helium are investigated. A vacancy is introduced into the simulation cell and the system is minimised using a conjugate gradient algorithm, yielding a single vacancy formation energy E_{vac} of 1.72 eV. Next, the atom with the highest potential energy is removed from the system and again the system is minimised. This scheme is iteratively continued to create voids up to the number of target vacancies and the formation energy of each is calculated. Next, helium atoms are introduced to the vacancies. The total system energy is measured and recorded. At this point, a Metropolis MC scheme [29] is used to find the low energy configurations. Every helium in the system is randomly displaced from its site up to a maximum of r_{max} (4.5 Å, the cut off distance for He–He interactions) in each of the x, y and z directions and then minimised using the conjugate gradient algorithm. Each bubble is continued for a minimum of 10,000 steps. After that, the searches will be terminated if the system energy does not drop within a further 10 steps. A schematic of this iterative process is shown in Fig. 1.

2.2. Cascade simulations near bubbles

For the cascades simulations the system is first thermalised before a cascade event is initiated. We choose a value of 500 K for the system temperature. After that a 1 keV cascade is initiated near the bubble, by imparting 1 keV energy to a primary knock-on

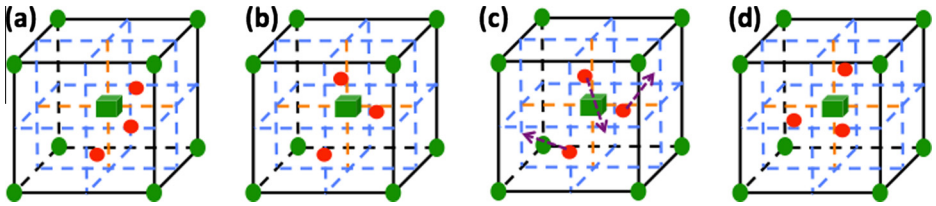

Fig. 1. The process is shown for He_3V_1. First, He atoms are randomly inserted (a) and then minimised (b). Next, He atoms are displaced randomly in the *x*, *y*, *z* directions (c) and minimised multiple times. The final configurations are determined from the lowest energy of the minimised structures (d). The He atoms are shown as red spheres and Fe atoms are green. The green cube is the vacancy of the bcc Fe cell. (For interpretation of the references to colour in this figure legend, the reader is referred to the web version of this article.)

atom (PKA). 1 keV is chosen because it is sufficiently large to cause well separated vacancies and interstitials and generate good statistics but not so large that the computations become infeasible.

To analyse the results of cascade simulations it is necessary to define an interaction region close to the bubble. We arbitrarily take this as a shell around the bubble up to the sixth nearest neighbour distance in the perfect bcc lattice. If an Fe vacancy or interstitial is created in this region, the cascade is defined as having interacted with the bubble. Fig. 2 illustrates this idea.

The probability of the cascade to cause damage in the interaction region is dependent on three factors: *d*, *s* and the direction of the cascade. For each chosen value of *s* and each bubble size, 8000 1 keV collision cascades were initiated in order to generate good statistics. The results are reported in Section 3.

2.3. He diffusion

To determine whether an isolated He atom or small He cluster will either form a seed point for a bubble or diffuse and join with an existing bubble it is necessary to evaluate the energy barriers for diffusion both in the bulk lattice and in the interaction region. Energy barrier calculations have been determined in two ways, either by using the nudged elastic band method (NEB) [30], when the final transition state is known or by searching for the saddle points from the local minimum energy state without knowing the final configurations [31,32]. We employ both methods here and have used the NEB method to check the barrier heights calculated on-the-fly. The rate for each transition is calculated using the Arrhenius equation:

$$\text{Rate} = \nu \cdot exp(-E_b/k_BT), \tag{4}$$

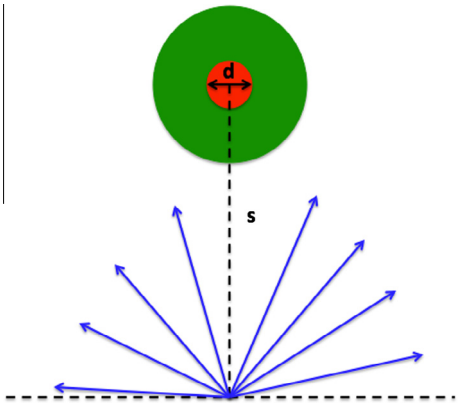

Fig. 2. The red region represents the He bubble and the green region defines the volume where we are interested in observing damage. *d* is the diameter of the bubble, *s* is the distance between the centre of the bubble and the position of the primary knock-on atom (PKA). The trajectories of the cascade are chosen over the half sphere. (For interpretation of the references to colour in this figure legend, the reader is referred to the web version of this article.)

where E_b is the energy barrier, ν is the transition prefactor, here assumed constant and taken to be 10^{13} s^{-1}; k_B is Boltzmann constant and T is the temperature.

To investigate the typical energy barrier for an isolated He to diffuse towards or outwards from an existing bubble, we classified He interstitials according to the distance between the interstitial and the surface of a bubble as given in Table 1. For each neighbour, at least 20 different positions of interstitials are investigated and 4000 on-the-fly barrier calculations carried out.

The results for the energy barriers shown in Section 3 are the lowest energies that were found among the transitions events.

3. Results and discussion

3.1. Formation energy

Fig. 3 shows the formation energy of the He_nV_m clusters calculated from the selected potentials at 0 K; each curve has a fixed number of vacancies, which implies that all the bubbles locating on the same curve have the preformed vacancies before He is inserted. To ensure the results can be compared on a similar scale, the figure shows the formation energy per vacancy. It is clear that each curve reveals the same trend; that is to say there is an optimal (lowest formation energy per vacancy) He-to-vacancy ratio for each curve. The corresponding bubble sizes can be found from the minima on the curves in Fig. 3. It can be seen that the optimum ratio increases from around 1:1 for small bubbles up to more than 4:1 for large bubbles. The curves show that even after the

Table 1
Classification of He interstitials with respect to the distance from an He bubble.

Neighbour (N)	1	2	3	4	5	6
Distance (Å)	1.0–1.9	1.9–2.8	2.8–3.5	3.5–4.2	4.2–5.1	5.1–6.0

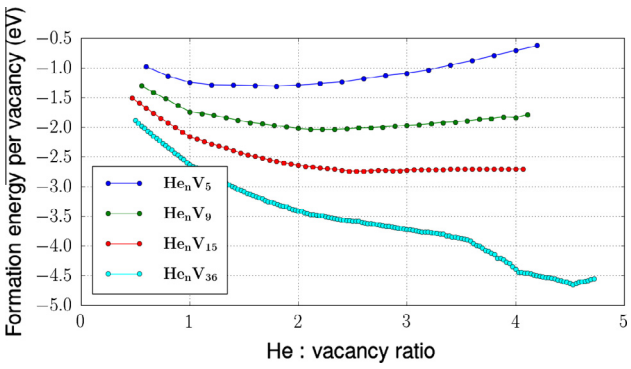

Fig. 3. The formation energy as a function of the number of helium atoms for different sizes of He_nV_m clusters.

minimum has been reached the formation energy is negative so more He could be added to the bubble. However this process cannot be continued beyond the ends of the curves shown because the bubbles cannot absorb more He so that the curves do not rise further than shown in the figure. The bubble sizes, calculated at the minimum, were found to be consistent with the work done by Caro et al. [10].

3.2. He clustering and bubble formation

To investigate how helium atoms can form clusters or bubbles, first we randomly distribute helium interstitials into a pure bcc Fe system and evolve the system using MD. This is similar to the methodology employed by Yang et al. Different concentrations of helium atoms are selected for comparison. The temperature of the system is set at 500 K. The system is then evolved for up to 5 ns.

From Fig. 4, we can see that most of the helium atoms accumulate into clusters over nanosecond time scales. Furthermore, the system is observed to change very little between 4 and 5 ns. We find that isolated helium atoms are highly mobile and aggregate into clusters. Some typical He clusters and bubbles are labelled in Fig. 4. Here we define a bubble as an He cluster with an associated vacancy. We can see the helium clusters with a size bigger than 3 can evolve into the helium bubbles. As found by Yang et al. [22], once the vacancy is formed, the configuration becomes unmovable over MD time scales.

The resultant isolated He and small He clusters diffuse to form large clusters or bubbles. Larger He complexes form by 5 ns. e.g. there is a $He_{10}V_2$ complex in Fig. 4(a) and (b). In addition, we can see Fe split interstitials around He_5V_1 and He_6V_1 in (a) and (b) of Fig. 4.

We also find the concentration of the helium in the Fe system plays a non-negligible role on the formation of the He clusters

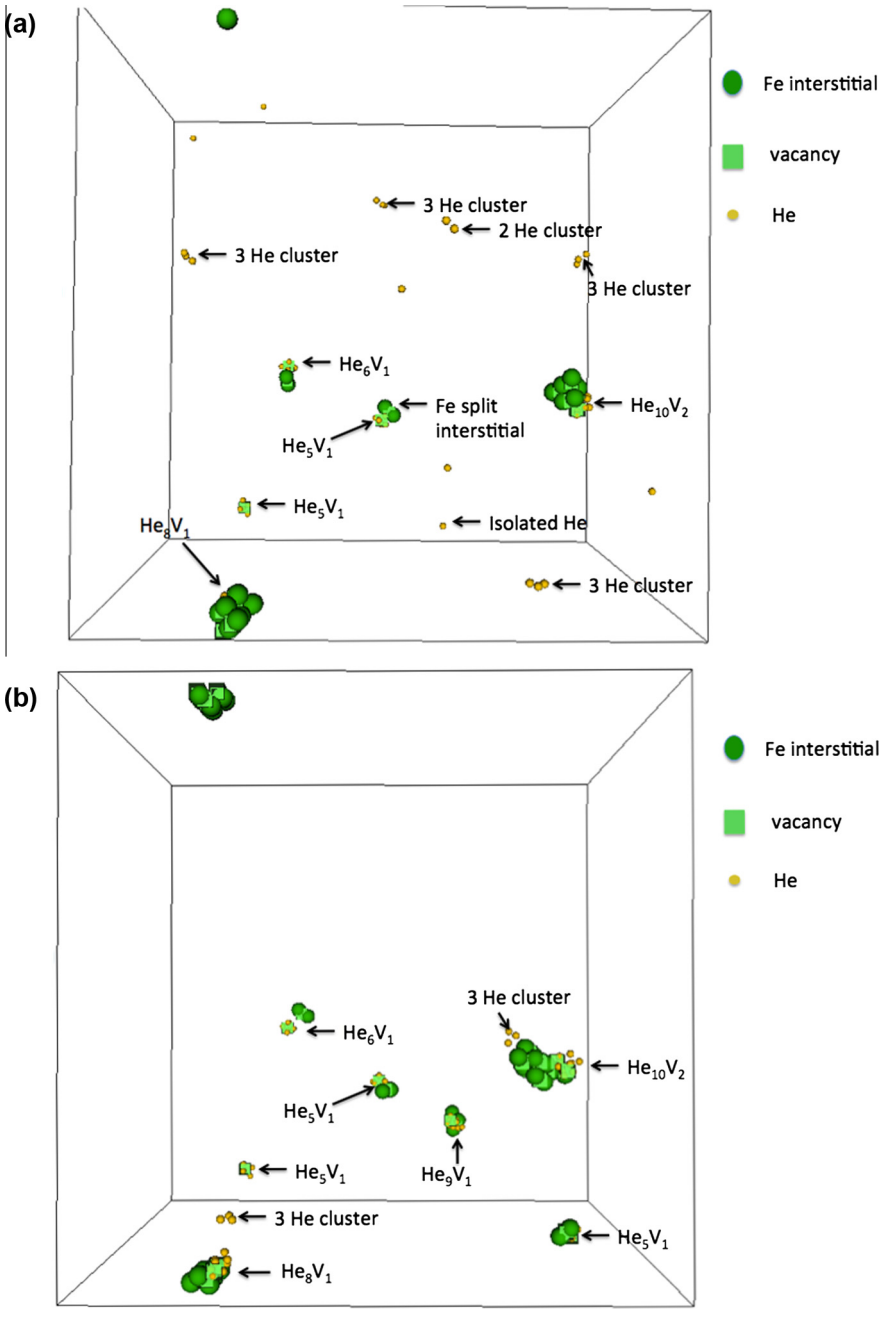

Fig. 4. The MD simulation of the bcc Fe system with randomly distributed He (0.1% concentration) at 1 ns and 5 ns.

and bubbles. As the concentration increases, large He bubbles (containing more than 10 He and more vacancies) appear within 1 ns (see Fig. 5).

The energy barrier for a single interstitial helium to diffuse is calculated as 0.06 eV. This shows that single helium is highly mobile at 500 K and therefore the diffusion is observable on MD time scales. The isolated He interstitial is located at a tetrahedral site. Diffusion occurs along the pathway from one tetrahedral site to its neighbouring tetrahedral site. In fact, by calculating the formation energy, single helium prefers to be substitutional rather than interstitial but this requires the vacancy pre-exists so that the He will instantly fall into the site since the energy barrier for an helium interstitial to occupy the site, emitting an Fe dumbbell is 6.76 eV as shown in Table 2. Thus an isolated He produced by a nuclear reaction would actually form as a tetrahedral interstitial in the first instance.

The He complexes that form from clustering at 500 K contain fewer vacancies than the He bubbles whose energies are plotted in Fig. 3. For these bubble sizes that are optimum at 0 K, larger energy barriers need to be overcome to form them. This point is discussed in more details in the next section.

The energy barriers of some typical transitions observed in the MD simulations have been calculated and these are summarised in Table 2. Diffusion of He clusters is found for clusters containing 2–4 He. But the mobility of the cluster decays as the size increases. When the size reaches 5 He, the trap mutation process occurs and an Fe atom is displaced into an interstitial position and the cluster becomes pinned. The displacement of an Fe atom can also happen for the cluster of 4 He but recombination can also occur. The typical energy barrier for this is 0.3 eV (i.e. the time scale for a hop at 500 K is about 11 ps) shown in Fig. 6. Having attained the shared vacancy position, the cluster can evolve further by forming a split interstitial with an energy barrier of 0.55 eV. The two-stage reverse process needs to overcome barriers of 0.4 eV and 0.013 eV respectively (see Fig. 6). This phenomenon of Fe ejection observed in MD simulation was never observed for clusters of size <4 since the energy barriers are too high.

Table 2
The typical energy barrier for He clusters to diffuse, to eject an Fe atom into an interstitial site and to take over one vacancy.

Typical energy barrier (eV)	He	He_2	He_3	He_4	He_5
To diffuse	0.06	0.12	0.2	0.48	–
To produce a ⟨1 1 0⟩ Fe dumbbell interstitial	6.76	5.65	4.52	0.55	0.13

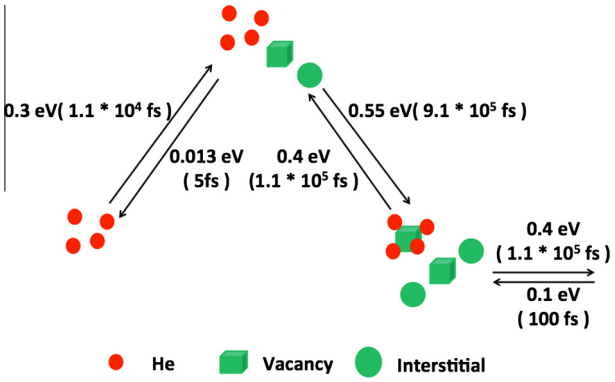

Fig. 6. Typical transitions for He_4 at 500 K.

As noted, the He_5 clusters can spontaneously eject an Fe atom into an interstitial position (see Fig. 7). The barrier for the Fe atom to recombine is 0.3 eV (i.e. the time scale for a hop at 500 K is about 11 ps), which shows the vacancy-free cluster is no longer the lowest energy state. Different from the situation for the He_4 cluster, it needs only 0.13 eV (i.e. the time scale for a hop at 500 K is about 210 fs) to take over this vacancy and form an Fe split interstitial. On the other hand, the energy barrier for the Fe interstitial to recombine back into the cluster is 0.4 eV, which is larger than the barrier to diffuse in the Fe lattice. (i.e. the time scale for a

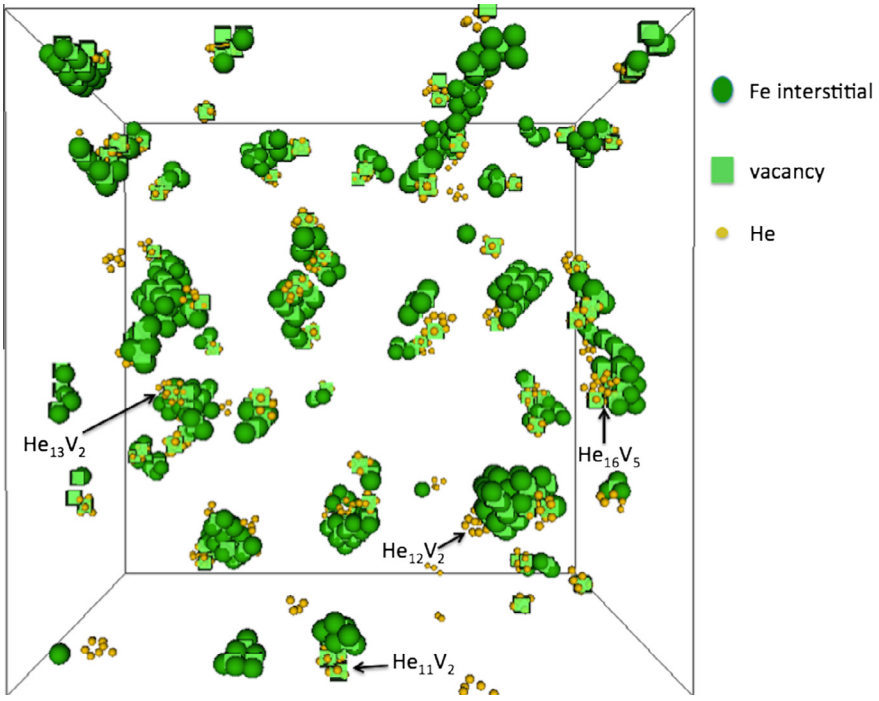

Fig. 5. The MD simulation of the bcc Fe system with randomly distributed He (1% concentration) at 1 ns.

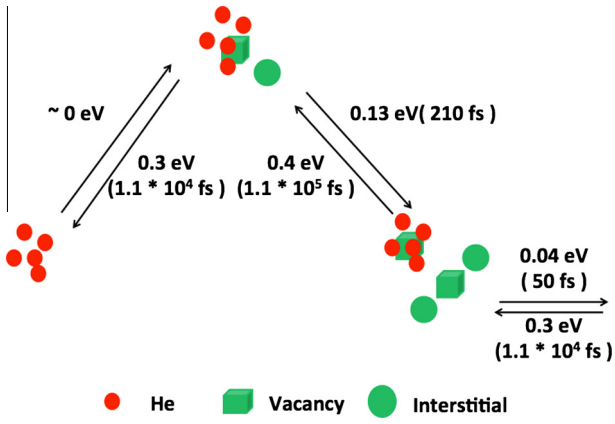

Fig. 7. Typical transitions for He_5 at 500 K.

hop at 500 K is about 0.11 ns), which implies that He_5 cluster prefers to evolve into an He bubble. When an He_5 cluster has created a vacancy and a split interstitial, the He_5V_1 system is observed to be stable over MD time scales and the cluster of 5 He atoms becomes the seed point of He bubble formation at 500 K.

The binding energy $E_{binding}$ of the small clusters was also calculated as defined below, in order to study the stability of these clusters.

$$E_{binding} = E_{system} - E_{Fe} \cdot N_{Fe} - E_{He} \cdot N_{He}, \quad (5)$$

where E_{He} is the formation energy of a helium tetrahedral interstitial and E_{Fe} is the cohesive energy of Fe, N_{Fe} and N_{He} refer to the number of Fe and He atoms in the system.

The binding energy of the smallest He clusters is shown in Table 3.

The negative value means that it is energetically favourable for helium to be in the cluster rather than stay isolated. The increasing binding energy per He atom shows stronger stability for larger He clusters. The small binding energy for the He_2 cluster and He_3 cluster implies the possibility of separation and thus we have examined the migration barriers for the separation of the small He clusters (see Table 4).

He interstitials can amalgamate into the small clusters (<4 He) in different ways. All of the forward barriers calculated were less than 0.2 eV, whereas the reverse barriers shown in Table 4 are much larger, thus indicating that it is kinetically favourable for the small He clusters to remain intact rather than separate. However, separation is also possible at 500 K over MD time scales.

Table 3
The binding energy of the He clusters for the lowest energy configurations.

	He_2	He_3	He_4	He_5
Binding energy per He atom	−0.125 eV	−0.236 eV	−0.317 eV	−0.37 eV

Table 4
The energy barrier for the small He clusters to separate.

Separation	He_2	He_3	He_4
He + He	0.3 eV		
He + He_2		0.48 eV	
He + He_3			0.6 eV

3.3. Collision cascades

To investigate the mechanism by which an He bubble may be enlarged, we examine the increase/decrease in Fe vacancies in the bubble by averaging over all generated cascades. The procedure is shown in Fig. 8. Fig. 8 shows some typical positions and directions of the cascades for three different sizes of He bubble. Fig. 8 also gives the cone angle within which the generated cascades will cause vacancies to form in the bubble and interaction region with a probability of 98%. Each cone is determined by generating 8000 separate cascade simulations.

For the larger bubbles, no interaction with the cascade will occur if the PKA is generated more than 6 nm from the bubble. For the small bubble this distance drops to 4.4 nm. By targetting the trajectories within the cones, statistics can be obtained without the necessity for lots of redundant trajectory calculations which produce no damage near the bubble.

Fig. 9 shows how the number of vacancies in the cluster changes, for the three sizes of He–vacancy clusters, where the initial number of vacancies is kept constant at 15. As might be expected, at a low He-to-vacancy ratio, emission of vacancies is clearly favoured. This changes at the optimal (from Fig. 3)) He-to-vacancy ratio, where the bubble absorbs vacancies. Above this ratio, vacancy capture becomes more favoured. Fig. 10 shows a typical example of the processes which occur in a typical collision cascade. Therefore, radiation provides a process for an He bubble to be enlarged by attracting vacancies.

3.4. Energy barriers for isolated He to join an existing bubble

In order to gain an understanding of He accumulation into bubbles, a study was carried out to investigate the energetics of the barriers for He to diffuse into an existing bubble from an interstitial site in the interaction region defined earlier (see Table 1). The migration energy barriers were calculated for the He interstitials diffusing towards He bubbles of different sizes. The initial positions of the interstitial He atoms were varied from 1 to 6 nearest neighbour distant from the edge of the bubble and the summarised data is presented in Table 5.

Typically He interstitial jumps occur to adjacent neighbour positions, e.g. if an He interstitial is initially positioned at 6N, then diffusion occurs by jumping to 5N, then from 5N to 4N and so on, until from 1N the He interstitial joins the bubble configuration. Therefore in Table 5 we give migration barriers for jumping to adjacent N position in the direction towards the bubble.

A barrier of 0 eV accounts for the cases when He interstitials instantaneously join the He bubble, during minimisation (or where the calculated barrier is less than 0.01 eV which implies the corresponding hop time is less than 50 fs). It usually occurs in the systems which consist of He bubbles which have a fairly low He-to-vacancy ratio (typically less than 3:1). This suggests that bubbles with a low He-to-vacancy ratio have a strong tendency to attract He interstitials that are in their vicinities.

An opposite behaviour was also observed for the cases with bubbles with a high He-to-vacancy ratio ($\geqslant$4:1). As can be seen in Table 5, with a growing He-to-vacancy ratio the migration barrier heights to jump towards a bubble increase, suggesting a loss of attraction to He interstitials. To investigate this effect and to complement the previous results, a similar study was performed by checking the migration barriers of He interstitials in the direction away from the bubble. This is summarised in Table 6.

He interstitials move from 1N to 2N, from 2N to 3N and so on as given in Table 6. The "–" accounts for the cases when no valid migration processes of He interstitials were observed because of instantaneously joining the bubble in these cases.

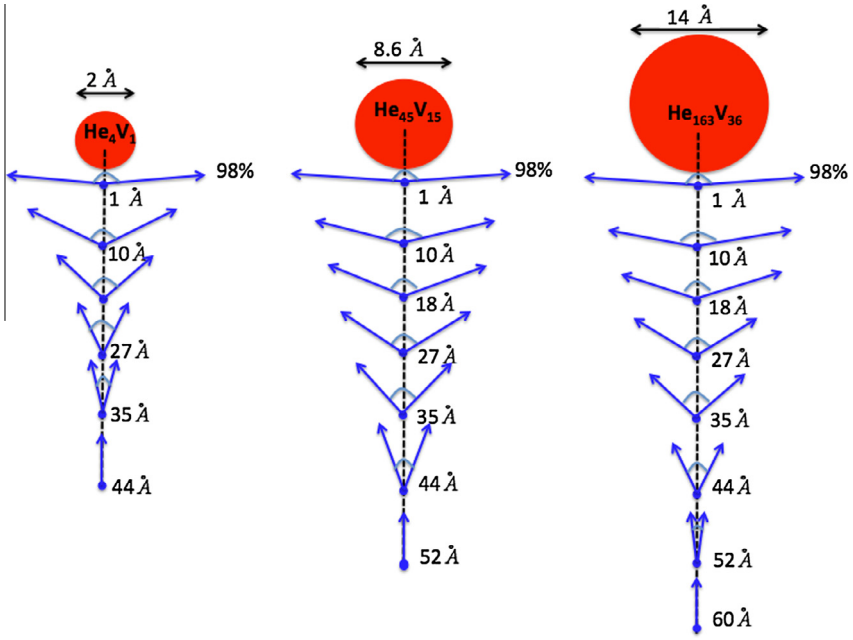

Fig. 8. Representations of the cones for collision cascades that have a 98% probability of interacting with the helium bubble. Different lines represent the cone angle as a function of separation and bubble size.

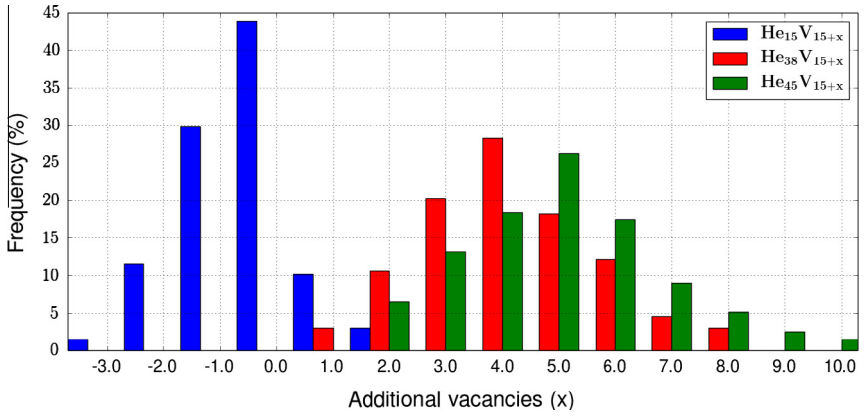

Fig. 9. Frequency of capture/loss of vacancies during the collision cascade for a system containing 15 vacancies. The three sets of results show three cases of (1) below the ideal (lowest energy in Fig. 3) He-to-vacancy ratio, (2) at the ideal ratio and (3) above the ideal ratio.

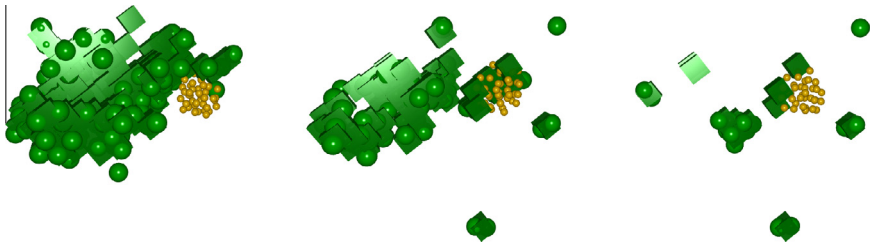

Fig. 10. Three frames in the MD simulation of a collision cascade near an $He_{38}V_{15}$ complex. The left image is after 100 fs, just as the cascade reaches the bubble, which remains in the same structure as at 0 fs; the centre image is after 1200 fs when the cascade has passed into the bubble and the right figure is the state after 10 ps, which shows the vacancies (green cubes in the figure) absorbed by the He bubble (the small yellow spheres). Split Fe interstitials can also be observed. (For interpretation of the references to colour in this figure legend, the reader is referred to the web version of this article.)

Table 6 also shows indications of a region around He bubble where an He atom is repulsed by a bubble by having a migration barrier to jump away from it lower than the barrier to jump towards the bubble; see the cases containing 15 vacancies in Tables 5 and 6. This is especially clear when bubbles have a high He-to-vacancy ratio ($\geqslant$4:1).

The data also indicates that even though the bubbles may have a ratio above the optimal (lowest energy from Fig. 3) configuration, they still can be enlarged in size, since most of the barriers are only slightly higher compared to the He interstitial migration barrier in pure Fe. See, e.g. the $He_{38}V_{15}$ case. For the cases with a high ratio, the migration barrier to move away from the bubble is lower than

Table 5
A summary of migration barriers (eV) of He interstitials diffusing towards He bubbles of different configuration. The first column specifies the bubble size, where the following columns represent the initial He interstitial position as specified in Table 1.

Typical energy barrier (eV)	Diameter (Å)	1N	2N	3N	4N	5N	6N
He_nV_5 ($n < 20$)	<6.3	0	0	0	0	0	0
$He_{20}V_5$	6.5	0	0	0	0.05	0.06	0.09
He_nV_9 ($n < 27$)	<7.5	0	0	0	0	0	0
$He_{27}V_9$	7.6	0	0	0	0	0	0.019
$He_{36}V_9$	8.4	0.004	0.006	0.016	0.04	0.06	0.08
He_nV_{15} ($n < 30$)	<7.6	0	0	0	0	0	0
$He_{30}V_{15}$	7.8	0	0	0	0.02	0.055	0.033
$He_{38}V_{15}$	8.0	0	0	0.03	0.018	0.1	0.099
$He_{45}V_{15}$	8.6	0	0.031	0.035	0.048	0.132	0.126
$He_{60}V_{15}$	9.8	0.006	0.02	0.087	0.087	0.08	0.08
He_nV_{36} ($n < 72$)	<10.2	0	0	0	0	0	0
$He_{72}V_{36}$	10.3	0	0	0.005	0.013	0.013	0.051
$He_{108}V_{36}$	11.4	0	0	0.004	0.039	0.036	0.017
$He_{144}V_{36}$	13	0	0	0.65	0.091	0.098	0.051
$He_{163}V_{36}$	14	0	0	2.542	1.6	0.273	0.1
$He_{98}V_{98}$	10.5	0	0.01	0.06	0.058	0.06	0.052
$He_{196}V_{98}$	12	0	0.029	0.07	0.024	0.023	0.02
$He_{294}V_{98}$	13.8	0	0.013	0.07	0.113	0.033	0.05
$He_{392}V_{98}$	16.2	0	1.619	0.709	0.3	0.148	0.047
$He_{169}V_{169}$	11	0	0.0065	0.01	0.046	0.06	0.05
$He_{338}V_{169}$	12.5	0	0.008	0.086	0.062	0.066	0.056
$He_{507}V_{169}$	16.5	0	0	1.699	0.332	0.170	0.036
$He_{676}V_{169}$	20	0	0	2.423	0.991	0.404	0.263

Table 6
A summary of migration barriers (eV) of He interstitials diffusing away from the He bubble. The first column specifies the bubble size and the following columns represent the initial He interstitial position as specified in Table 1.

Typical energy barrier (eV)	1N	2N	3N	4N	5N	6N
$He_{27}V_9$	–	–	–	–	–	2.109
$He_{36}V_9$	1.8	0.01	0.02	0.06	0.08	0.12
$He_{30}V_{15}$	–	–	–	1.9	0.061	0.041
$He_{38}V_{15}$	–	–	2.0	0.007	0.046	0.045
$He_{45}V_{15}$	–	2.2	0.01	0.001	0.064	0.052
$He_{60}V_{15}$	2.2	0.01	0.007	0.069	0.02	0.05
$He_{72}V_{36}$	–	–	2.2	0.008	0.019	0.076
$He_{108}V_{36}$	–	–	2.6	0.009	0.006	0.007
$He_{144}V_{36}$	–	–	0.110	0.025	0.07	0.04
$He_{163}V_{36}$	–	–	0.001	0.005	0.009	0.003
$He_{98}V_{98}$	–	3.4	0.09	0.064	0.062	0.061
$He_{196}V_{98}$	–	2.66	0.039	0.021	0.02	0.02
$He_{294}V_{98}$	–	2.645	0.045	0.018	0.025	0.026
$He_{392}V_{98}$	–	0.023	0.066	0.02	0.034	0.021
$He_{169}V_{169}$	–	3.531	0.03	0.056	0.065	0.06
$He_{338}V_{169}$	–	3.533	0.086	0.051	0.06	0.047
$He_{507}V_{169}$	–	–	0.027	0.012	0.014	0.007
$He_{676}V_{169}$	–	–	0.02	0.012	0.006	0.006

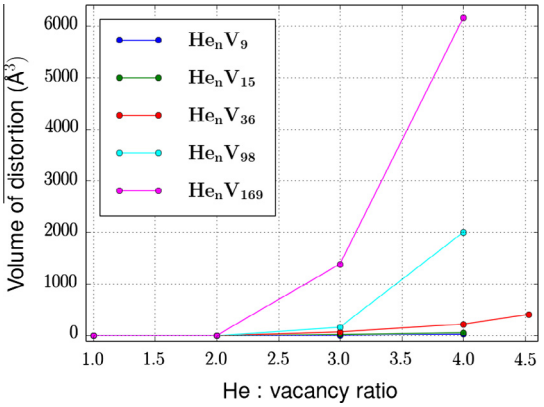

Fig. 11. The volume of distortion as a function of the number of helium atoms for different sizes of He_nV_m clusters. For the $He_{163}V_{36}$ bubble, the volume of 400 Å^3 corresponds to an annular region around the bubble of between 2 and 3 Å in width.

the one to jump towards it, as in the $He_{45}V_{15}$ case. Once the He interstitial joins into the bubble, it cannot leave the bubble because of the huge barrier.

Further, if we investigate the bubbles with 36 vacancies, for the lower He-to-vacancy ratio (<2:1), jumping into the bubble happens instantaneously for the He interstitial at 6th neighbour. For the bubbles with ratios between 2:1 and 3:1, it is kinetically favourable for additional He to join as the migration barrier is lower than the diffusion barrier in pure Fe. However, the barrier to jump away becomes lower than the barrier to jump in when the ratio is more than 3:1. When the bubble attains a 4:1 ratio, there is a big energy barrier for He to jump from the 3rd neighbour. This is even more clear when the bubble reaches the optimal (from Fig. 3) configuration. In these cases, it is kinetically favourable for the He interstitial to stay outside the bubble. Similar conclusions can also be drawn for the larger He bubbles e.g. He_nV_{98} and He_nV_{169} in Tables 5 and 6. In the case of He_nV_{98}, only when the He-to-vacancy ratio is 1:1, well below optimal (from Fig. 3), is it more favourable for the He atom to diffuse towards the bubble than to diffuse away.

In summary, for the bubbles with the diameter $\lessapprox$11 Å, it is kinetically possible to absorb additional He, even when the He-to-vacancy ratio is above that corresponding to the minimum energy shown in Fig. 3. This might be expected since the energies shown in Fig. 3 are still negative, but the He interstitial becomes less likely to jump towards the bubble when the diameter $\gtrapprox$9 Å and the He-to-vacancy ratio $\geqslant$3:1. Isolated He diffusion into bubbles with a diameter >13 Å and the He-to-vacancy ratio >4:1 occurs only very infrequently at room temperature.

One of the reasons that the larger bubbles find it more difficult to absorb He is the strain and distortion introduced into the Fe lattice. We can calculate the volume of material around a bubble in which the Fe atoms are displaced from their lattice sites. If we (arbitrarily) calculate this region as the region in which the atoms are displaced by at least one third of the nearest neighbour distance, Fig. 11 shows that this volume increases non-linearly with bubble size.

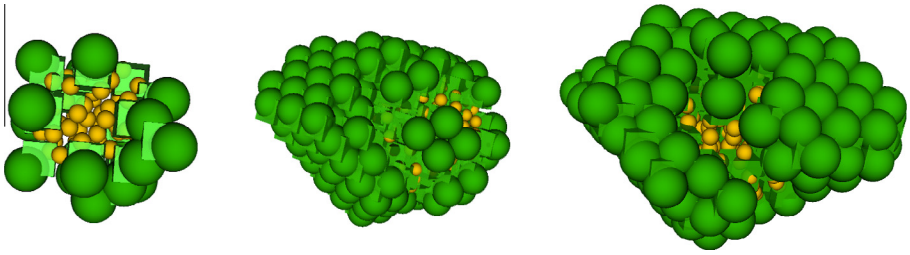

Fig. 12. The distortion around the bubble $He_{60}V_{15}$, $He_{144}V_{36}$ and $He_{163}V_{36}$.

Fig. 12 shows the strained region for bubbles containing 36 vacancies. The region is not spherical in shape but as with Fig. 11 it indicates that the strained region grows rapidly with increasing bubble size so there appears to be a direct correlation between the lattice strain and the energy barriers for isolated He to diffuse into the bubble.

4. Conclusions

Single helium atoms prefer to be substitutional rather than interstitial but the energy barrier for this to occur is large. Thus an isolated He atom injected into a bcc Fe lattice would be expected to be located at a tetrahedral site. The He interstitial can diffuse quickly in the bcc Fe system with a pathway between adjacent tetrahedral sites. These highly mobile He interstitials lead to He clustering. He_n, $n = 1, 2, 3$ clusters are also mobile over MD time scales at 500 K but a cluster of 5 He can eject an Fe interstitial and become the seed point for less mobile bubbles. These less mobile bubbles can initially continue to grow through the attraction of He_n, $n = 1, 2, 3$ clusters. The optimal (from Fig. 3)) He-to-vacancy ratio has been determined and it has been shown how bubbles can also absorb additional vacancies produced by irradiation to reduce the lattice strain around the bubble, which would reduce the energy barriers and allow more He to join. The energy barriers for a diffusing He atom to join an existing bubble have been shown to increase rapidly as the size of the bubble increases and the strained region around the bubble increases in size. Thus the Ostwald ripening process becomes kinetically limited as the size of the bubble grows. These results are in good agreement with the experimental work of [9] in pure Fe which show that bubbles of between 1 and 2 nm in diameter are preferentially formed at room temperature.

Acknowledgements

The main part of the work was carried out as part of the EPSRC funded PROMINENT project, Performance and Reliability of Metallic Materials for Nuclear Fission Power Generation, Grant EP/I003274/1.

References

[1] S.J. Zinkle, Phys. Plasmas 12 (2005) 058101.
[2] R. Kurtz, A. Alamo, E. Lucon, Q. Huang, S. Jitsukawa, A. Kimura, R. Klueh, G. Odette, C. Petersen, M. Sokolov, P. Spätig, J.-W. Rensman, J. Nucl. Mater. 386–388 (2009) 411–417.
[3] G. Lucas, R. Schäublin, J. Phys.: Condens. Matter 20 (2008) 415206.
[4] P.J. Maziasz, J. Nucl. Mater. 205–205 (1993) 118–145.
[5] S.J. Zinkle, P.J. Maziasz, R.E. Stoller, J. Nucl. Mater. 206 (2008) 266–286.
[6] T. Yamamoto, G.R. Odette, P. Miao, D.J. Edwards, R.J. Kurtz, J. Nucl. Mater. 386–388 (2009) 338–341.
[7] K. Ono, J. Nucl. Mater. 307–311 (2010) 1507–1512.
[8] J. Henry, L. Vincent, X. Averty, B. Marini, P. Jung, J. Nucl. Mater. 367–370 (2007) 411–416.
[9] K. Yu, Y. Liu, C. Sun, H. Wang, L. Shao, E. Fu, X. Zhang, J. Nucl. Mater. 425 (2012) 140–146.
[10] A. Caro, J. Hetherly, A. Stukowski, M. Caro, E. Martinez, S. Srivilliputhur, L. Zepeda-Ruiz, M. Nastasi, J. Nucl. Mater. 418 (2011) 261–268.
[11] A. Caro, D. Schwen, E. Martinez, Appl. Phys. Lett. 103 (2013) 213115.
[12] N. Gao, H. Van Swygenhoven, M. Victoria, J. Chen, J. Phys.: Condens. Matter 23 (2011) 442201.
[13] Z. Di, X.-M. Bai, Q. Wei, J. Won, R.G. Hoagland, Y. Wang, A. Misra, B.P. Uberuaga, M. Nastasi, Phys. Rev. B 84 (2011) 052101.
[14] R. Stoller, S. Golubov, P. Kamenski, T. Seletskaia, Y. Osetsky, Philos. Mag. 90 (2010) 923–934.
[15] R. Stoller, Y. Osetsky, J. Nucl. Mater. 455 (2014) 258–262.
[16] D.M. Stewart, Y.N. Osetskiy, R.E. Stoller, MRS Proc. 1298 (2011) 79–83.
[17] T. Jourdan, J.-P. Crocombette, J. Nucl. Mater. 418 (2011) 98–105.
[18] S. Hafez Haghighat, R. Schäublin, Philos. Mag. 90 (2010) 1075–1100.
[19] E. Hayward, C. Deo, J. Phys.: Condens. Matter 24 (2012) 265402.
[20] D. Terentyev, N. Juslin, K. Nordlund, N. Sandberg, J. Appl. Phys. 105 (2009) 103509.
[21] D.J. Hepburn, D. Ferguson, S. Gardner, G.J. Ackland, Phys. Rev. B 88 (2013) 024115.
[22] L. Yang, H. Deng, F. Gao, H. Heinisch, R. Kurtz, S. Hu, Y. Li, X. Zu, Nucl. Instrum. Methods Phys. Res. Sect. B 303 (2013) 68–71.
[23] N. Gao, M. Victoria, J. Chen, H. Van Swygenhoven, J. Phys.: Condens. Matter 23 (2011) 245403.
[24] F. Gao, H. Deng, H. Heinisch, R. Kurtz, J. Nucl. Mater. 418 (2011) 115–120.
[25] G.J. Ackland, M.I. Mendelev, D.J. Srolovitz, S. Han, a.V. Barashev, J. Phys.: Condens. Matter 16 (2004) S2629–S2642.
[26] R.A. Aziz, A.R. Janzen, M.R. Moldover, Phys. Rev. Lett. 74 (1995) 1586–1589.
[27] X. Gai, R. Smith, S. Kenny, MRS Proc. 1514 (2013) 21–26.
[28] E. Hayward, C. Deo, J. Phys.: Condens. Matter 23 (2011) 425402.
[29] N. Metropolis, A.W. Rosenbluth, M.N. Rosenbluth, A.H. Teller, E. Teller, J. Chem. Phys. 21 (1953) 1087.
[30] G. Henkelman, H. Jonsson, J. Chem. Phys. 113 (2000) 9978.
[31] C. Scott, S. Blackwell, L. Vernon, S. Kenny, M. Walls, R. Smith, J. Chem. Phys. 135 (2011) 174706.
[32] S. Blackwell, R. Smith, S.D. Kenny, J.M. Walls, Phys. Rev. B 86 (2012) 035416.